IEEE Photonics Journal
An IEEE Photonics Society Publication

Tunable Electro- and All-Optical Switch Based on Epsilon-Near-Zero Metasurface

Volume 12, Number 4, August 2020

Ze Tao Xie
Jiaye Wu
H. Y. Fu
Qian Li

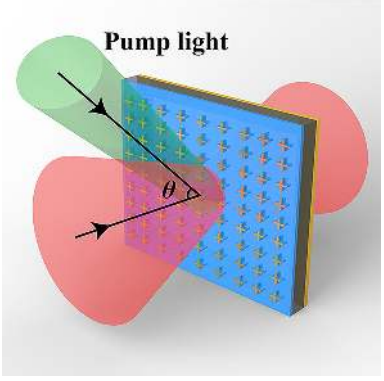

DOI: 10.1109/JPHOT.2020.3010284

IEEE photonics SOCIETY
IEEE

Tunable Electro- and All-Optical Switch Based on Epsilon-Near-Zero Metasurface

Ze Tao Xie,[1] **Jiaye Wu**,[1] **H. Y. Fu**,[2] **and Qian Li** [1]

[1]School of Electronic and Computer Engineering, Peking University, Shenzhen 518055, China
[2]Tsinghua-Berkeley Shenzhen Institute (TBSI), Tsinghua University, Shenzhen 518055, China

DOI:10.1109/JPHOT.2020.3010284

Manuscript received June 2, 2020; revised July 12, 2020; accepted July 15, 2020. Date of publication July 20, 2020; date of current version August 26, 2020. This work was supported in part by the National Natural Science Foundation of China under Grant 61675008, in part by Shenzhen Science and Technology Innovation Commission under Grant GJHZ2018411185015272 and JCYJ20170818094001391, and in part by Youth Science and Technology Innovation Talent of Guangdong Province (2019TQ05X227). Corresponding author: Qian Li (e-mail: liqian@pkusz.edu.cn).

Abstract: A novel design of a tunable optical switch based on epsilon-near-zero (ENZ) metasurface is proposed, which can work as an electro-optical or an all-optical switch, and be tuned by gate-voltages, incident angles, and intensity of pump light. The result shows that the coupling of the ENZ mode and plasmon resonance lead to an obvious Rabi splitting which can be observed in the transmission spectrum. Numerical analysis also demonstrates that the coupling belongs to the ultra-strong coupling regime. The proposed design can achieve electro-optical switching with a large modulation depth of up to $\sim$ 17 dB, all-optical switching with an extinction ratio exceeding 5 dB and an ultrafast response time of 650 fs.

Index Terms: ENZ material, intergrated optics devices, indium tin oxide, metasurface, optoelectronic materials, optical switch.

1. Introduction

Optical switches, as an essential component of optical logic gates and related devices, hold the key to on-chip ultrafast optical connection networks as well as integrated photonic circuits [1]. The current state-of-the-art design of optical switches includes photonic crystal nanocavities [2], [3], surface plasmon polaritons [4], metamaterials [5], [6], microring resonators [7], [8] and etc. Their outstanding performance include high switching efficiency and speed, low power consumption and integration size, as compared to traditional electronic switches. However, challenges stem from the materials of optical switches, including limited carrier densities (i.e., in silicon and indium arsenide), untunablity (i.e., in metals and dielectric), relatively narrow spectral range (i.e., graphene), low response speed, and complementary metal oxide semiconductor (CMOS) incompatibility [1], [9].

Recently, a novel class of materials with zero or near-zero permittivity at one or multiple wavelengths, known as epsilon-near-zero (ENZ) material, has become a research focus in photonics [10]–[13]. It has been reported that ENZ materials exhibit many extraordinary optical properties, including tunneling effects [14], transmission with constant phase [15], field enhancement [16], strong coupling phenomena [17] and large nonlinear responses [18], [19], etc. The ENZ material can be obtained in natural semiconductors or artificial metamaterials. Notably, transparent conducting oxides (TCOs) is one of the most widely used ENZ materials, due to its unique application potential.

TCOs allow flexible electron densities from 10^{19} to 10^{21} cm^{-3}, thus offer a wide ENZ response region from ultraviolet to near-infrared spectral range [20]. Its ENZ wavelength is strongly dependent on the electron densities, which can be tuned by applying electrostatic field [21] or optical pumping [18]. Among TCOs, indium tin oxide (ITO) is the most studied ENZ media for integrated photonics. ITO has revealed its advantages of tunability, CMOS compatibility, low cost, enhanced second- [22] and third-harmonic generation [23], ultrahigh nonlinear Kerr and ultrafast response [13], [19]. Until now, many potential applications arising from ENZ behavior of ITO have been proposed or demonstrated including perfect light absorber [17], [24], optical modulator [25], all-optical switch [26]–[28]. However, the aforementioned devices can only operate in one single function, either by applying different voltage or by optical pumping, which limits the application and potential of ITO in integrated optical devices.

In this work, we propose a tunable dual-function optical switch (electro-optical and all-optical) based on the epsilon-near-zero metasurface in the near-infrared region. The metasurface consists of a cross-shaped array of gold, to support surface plasmon resonance, enhance the electric field, and couple the normally incident light into the ENZ ITO material [12]. By incorporating the ENZ ITO material, an obvious Rabi splitting is present in the transmission spectrum, which denotes the coupling of the ENZ mode and plasmon resonance, and is crucial to the optical switching functionality. It is demonstrated that the proposed coupled system belongs to the ultra-strong coupling regime. Furthermore, this switch can be tuned by voltage bias, incident angles, and intensity of pump light. When operating as an electro-optical switch, a modulation depth of 8 dB to $\sim$17 dB can be obtained from 1.375 μm to 1.545 μm. While as an all-optical switch, the proposed dual-function switch can provide an extinction ratio (ER) exceeding 5 dB with an ultra-fast response time of about 650 fs. The performance of our proposed structure is on par with those reported recently (ER $=$ 20 dB for ENZ electro-absorption modulator [29] and ER $=$ 5.1 dB for ENZ all-optical modulator [25]). More importantly, the highlight of our proposed design is that it could be used as either an electro- or all-optical switch, bridging the two classes of optical switches for the first time.

This article is structured as follows. In Section 2, the structural design and the theoretical methods used are introduced. In Section 3, the physical mechanisms and the structural design analyses are presented. The performance of the proposed design as an electro-optical and an all-optical switch is analyzed in Section 4 and Section 5, respectively. The paper is concluded by Section 6.

2. Structural Design and Theoretical Models

Fig. 1(a) shows the three-dimensional (3D) schematic of the designed metasurface with ENZ ITO materials. The metasurface consists of a cross-shaped array of 100-nm thick gold (Au) and 23-nm thick ITO, with length, width, and periodicity of $W = 50$ nm, $L = 450$ nm, and $P_x = P_y = 900$ nm, respectively, and placed on a 4-nm thick ITO nanofilm and a substrate of hafnium dioxide (HfO_2) with a thickness of 50 nm. Opting for the high-k dielectric HfO_2 can provide a maximum amount of charge accumulation under the same bias voltage compared with other dielectrics. The hollow gold square underneath the substrate and ITO nanofilm functions as electrodes to apply different voltage V.

The complex relative permittivity of Au and ITO can be described by the Drude model [30]:

$$\varepsilon = \varepsilon_\infty - \frac{\omega_p^2}{\omega^2 + i\Gamma\omega}, \tag{1}$$

here, ε_∞ is the permittivity at the infinite frequency, ω is the angular frequency of incident light, $\omega_{\rm p}$ is the plasma frequency, and Γ is the Drude damping rate. It is worth mentioning that the plasma frequency $\omega_{\rm p}$ is a function of the electron density N:

$$\omega_p = \sqrt{\frac{Ne^2}{m_e^* \varepsilon_0}}, \tag{2}$$

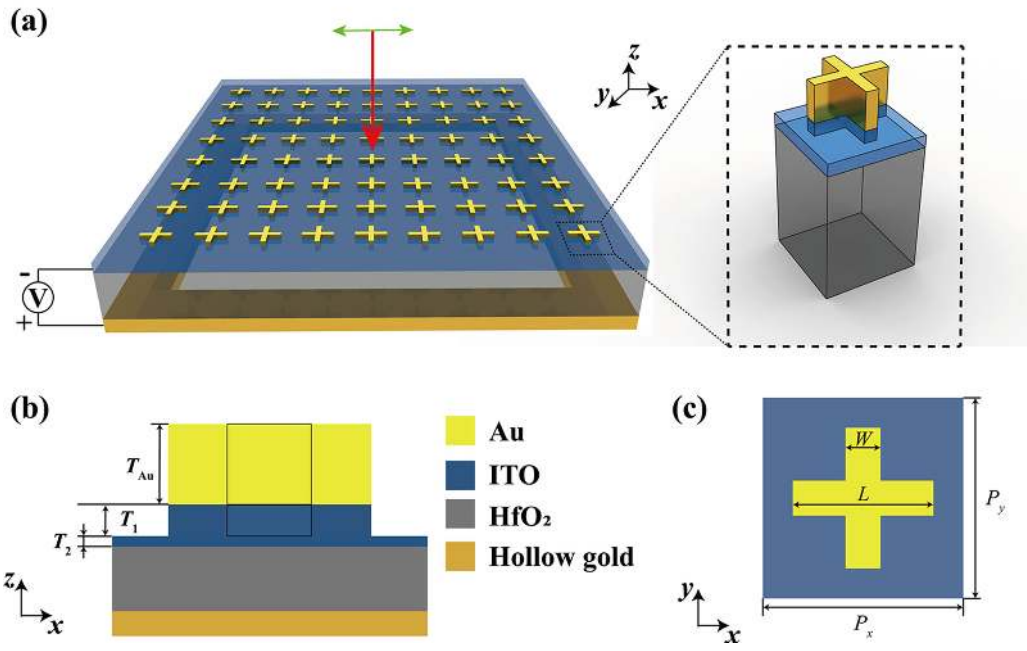

Fig. 1. (a) 3D schematic overview of the proposed structure, with a cross-shaped array of Au and ITO located on top of an ITO nanofilm on the HfO_2 substrate. An *x*-polarized plane wave normally incident on the metasurface. (b) Cross-sectional view of the structure in the *x*-*z* plane. The thickness of Au, cross-shaped ITO, and ITO nanofilm are $T_{\mathrm{Au}} = 100$ nm, $T_1 = 23$ nm, and $T_2 = 4$ nm, respectively. The HfO_2 substrate is 50 nm thick. (c) The unit cell structure of the design on the *x*-*y* plane. The length, width, and periodicity are $W = 50$ nm, $L = 450$ nm, and $P_x = P_y = 900$ nm, respectively.

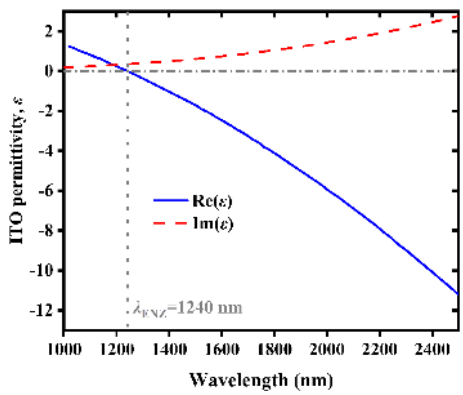

Fig. 2. The variation of the real (solid blue line) and imaginary parts (dashed red line) of the complex permittivity, as a function of the wavelength. Re(ε) vanishes at $\lambda_{\mathrm{ENZ}} = 1240$ nm.

with m_e^* the effective mass of the electron, e the charge of an electron, and ε_0 the vacuum permittivity.

We use experimental values for the Drude model parameters of Au and ITO. For Au, $\varepsilon_\infty = 1$, the plasma frequency $\omega_{\mathrm{p}} = 2\pi \times 2060 \times 10^{12}$ rad/s, the Drude damping rate $\Gamma = 2\pi \times 10.9 \times 10^{12}$ rad/s [31]. For ITO, $\varepsilon_\infty = 3.8055$, $\omega_{\mathrm{p}} = 2.97 \times 10^{15}$ rad/s, $\Gamma = 1.39 \times 10^{14}$ rad/s [18]. Fig. 2 shows the calculated result of the complex relative permittivity of ITO. The real part Re(ε) crosses zero at 1240 nm, indicating the ENZ wavelength of ITO is $\lambda_{\mathrm{ENZ}} = 1240$ nm. The finite-difference time-domain (FDTD) method (Lumerical FDTD solutions) is used to numerically analyze the optical

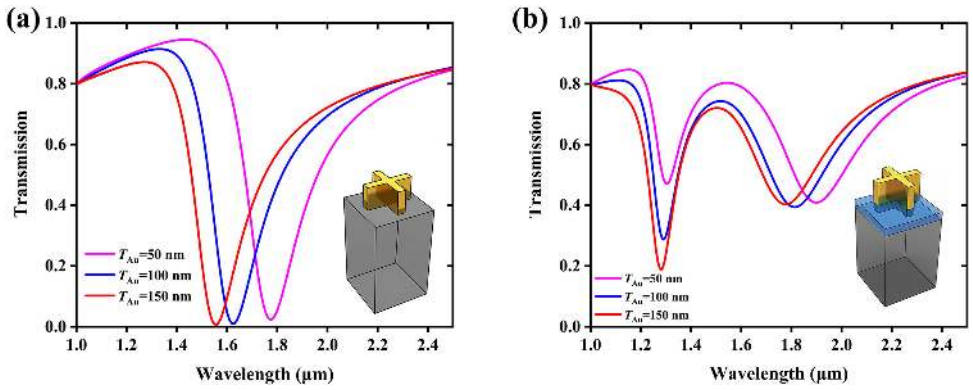

Fig. 3. Transmission spectra for metasurface (a) without and (b) with ITO at different T_{Au}. The schematic in each subfigure is the unit cell structure of the corresponding metasurface.

response of the proposed device. In the simulation, the perfectly matched layers (PML) absorbing boundary conditions are used in the *z*-direction, while the periodic boundary conditions are used in the *x* and *y* directions.

3. Physical Mechanisms and Structural Design Analyses

To explore the effect of ENZ ITO, we first calculate the optical response of the metasurface without and with ITO, respectively. Fig. 3(a) shows the transmission spectrum of the simple cross-shaped Au metasurface without ITO at different thickness T_{Au}. A clear dip can be observed in the spectrum, resulting from the plasma resonance of the cross-shaped Au excited by the incident light. It is clear that the plasma resonance is strongly dependent on the dimensions, increasing the thickness T_{Au} from 50 nm to 150 nm leads to a blueshift of the dip over 220 nm corresponding to 24 THz. In comparison, Fig. 3(b) shows the transmission curves for the device with ITO. The spectrum displays a Rabi splitting with two dips of different resonance strength at the short and long wavelengths, respectively, which is markedly different from that of the device without ITO. Furthermore, with the increase of T_{Au}, the long-wavelength dip is blue shifted, while the position of the short-wavelength dip remains almost unchanged within the ENZ zone. The main impact of the short-wavelength dip is a change in ER (which is defined as $-10\mathrm{Log}_{10}T$), which reduces about 45%. Therefore, the addition of ENZ ITO components are beneficial in forming the optical switching mechanism. This is further represented in Fig. 4 which map the evolution of the resonance as the T_{Au} changes over a large range. The black dashed line indicates the resonance wavelength of the simple cross-shaped Au metasurface without ITO. As seen from Fig. 4 that the position of the long-wavelength dip has a similar trend with the plasmon resonance of the metasurface without ITO, while the short-wavelength dip is pinned at $\sim$1.29 μm. Such result implies that in the transmission spectra of the device with ITO, the short-wavelength dip is related to the strong coupling of ENZ ITO, and the long-wavelength dip is dependent on the plasmon resonance.

Next, we simulate respectively the field distributions of |E| and |H| corresponding to the short-wavelength dip and the long-wavelength for $T_{\mathrm{Au}} = 100$ nm, to further investigate the physical mechanism of the observed resonances. For the short-wavelength dip at 1.29 μm, the |E| field is mainly distributed on the edge of Au, strongly enhanced and confined into the ENZ ITO, as shown in Fig. 5(a). Moreover, the |E| field abruptly ends at the interface of the ITO nanofilm and HfO_2 substrate, indicating the excitation of the ENZ mode [32]. For the |H| filed distribution, Fig. 5(d) shows that it is locally enhanced in the ITO, which is excited by the surface plasmon resonance. However, from Fig. 5(b), it can be observed that the |E| field distribution of the long-wavelength dip at 1.83 μm leaks to ITO-HfO_2 and HfO_2-Air interfaces, indicating a weak ENZ mode. The |H|

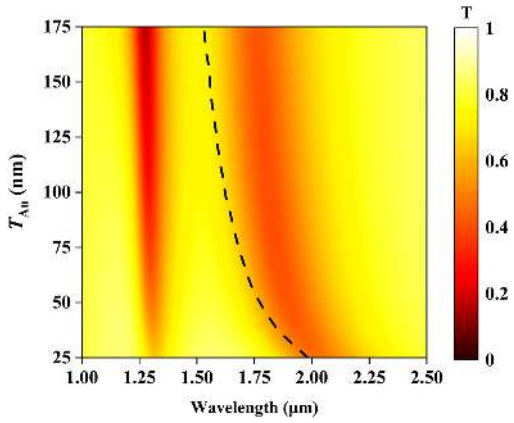

Fig. 4. Transmission spectra of the metasurface with ITO as a function of T_{Au}. The black dashed line indicates the plasmon resonance wavelength of the simple metasurface without ITO.

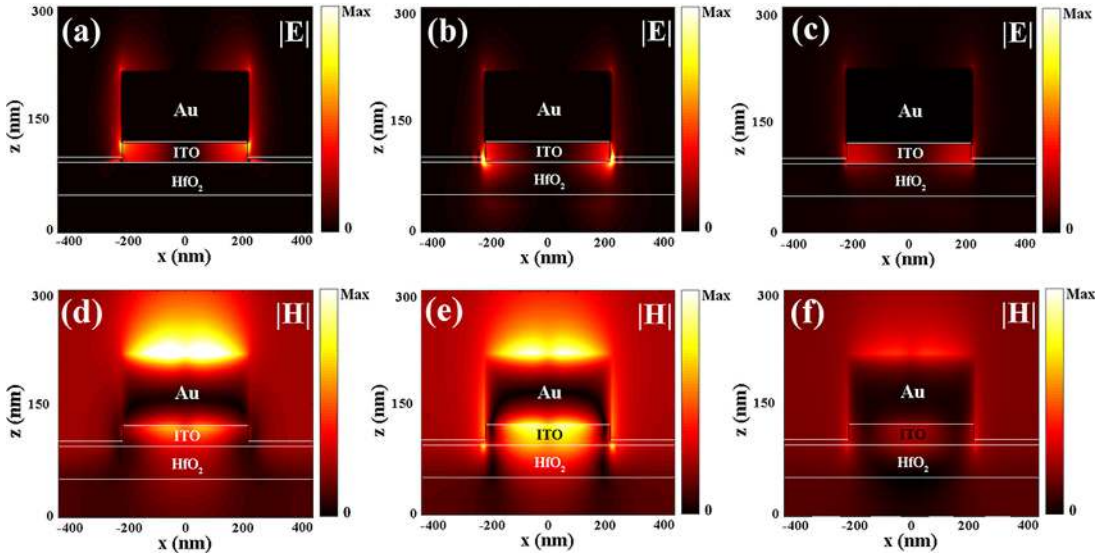

Fig. 5. The |E| field distribution for (a) short-wavelength dip at 1.29 μm, (b) long-wavelength dip at 1.83 μm, and (c) transmission peak at 1.55 μm. The |H| field distribution for (d) short-wavelength dip, (e) long-wavelength dip, and (f) transmission peak.

filed distribution (Fig. 5(e)) at the same wavelength has a more obvious local enhancement than that of the short-wavelength dip, owing to a stronger plasmon resonance. Figs. 5(c) and 5(d) are the field distributions of |E| and |H| of the transmission peak between the short-wavelength and long-wavelength (1.55 μm), respectively. The electric and magnetic field strength become weak compared to the short-wavelength dip and the long-wavelength dip. The light only weakly interacts with gold and ITO in this case, which indicates the absence of field enhancement and results in the strong transmission. Moreover, the field distributions of |E| at 1.55 μm has leaked to ITO-HfO_2 and HfO_2-Air interfaces with weak intensity, which is similar to the long-wavelength, meaning that ENZ mode gradually weakens from the short-wavelength to long-wavelength. The result reveals that the short-wavelength and long-wavelength dips are efficiently excited by the coupling between the ENZ mode and the plasmon resonance. It can be concluded that the ENZ mode and the plasmon resonance play a leading role in the short-wavelength and long-wavelength dips respectively. In

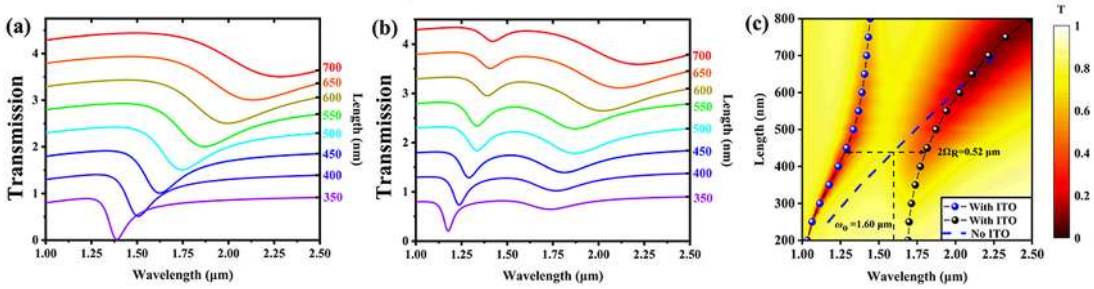

Fig. 6. Transmission spectra for (a) simple metasurface without ITO (bare cavity resonance) (a) and (b) metasurface with ITO (the coupled system). (a) and (b) show the transmission spectra for various *L*. Each spectrum is vertically shifted by 0.5 for clarity. (c) The evolution of the transmission spectra of the metasurface with ITO as a function of *L*. The curves with blue and black circles represent the short-wavelength and long-wavelength dip of the coupled system, and the blue dashed line represents the plasma resonance wavelength of the bare cavity resonance.

addition, from the field distributions of |E|, the unchanged position of short-wavelength resonance is the result of the strong interaction between the ENZ mode and the plasmon resonance [33].

To investigate the impact of the device's geometry, the case of changing the length *L* is also discussed. It is known that the optical response of antennas is strongly dependent on the dimensions under the situation that incident light polarized parallel to the antenna length [34]. Therefore, the different resonance of the structure can be observed with various *L*. Figs. 6(a) and 6(b) illustrate the transmission spectra of the simple metasurface without ITO (bare cavity resonance) and metasurface with ITO (the coupled system), respectively. Again, the plasma resonance and the Rabi-splitting are observed in each spectrum. Fig. 6(c) shows the evolution of the coupled system over a large varying range of *L*. The curves with blue and black circles represent the short-wavelength and long-wavelength dip from the coupled system, while the blue dashed line is the plasma resonance wavelength from the bare cavity resonance. When *L* is adjusted within the range of 200 nm to 800 nm, a clear anti-crossing pattern occurs at the blue and black circles lines, which characterizes the ultra-strong coupling [35]. Besides, the minimal splitting of the anti-crossing line of the coupled system is $2\Omega_{\mathrm{R}} = 0.52\ \mu$m for a cross-shaped length $L = 440$ nm, corresponding to the bare resonance wavelength $\omega_0 = 1.60\ \mu$m. According to the ultra-strong coupling condition $\Omega_{\mathrm{R}}/\omega_0 > 0.1$, a normalized coupling rate of $(\Omega_{\mathrm{R}}/\omega_0) = (0.26\ \mu\mathrm{m}/1.60\ \mu\mathrm{m}) = 0.1625$, placing the proposed ENZ ITO metasurface coupled system into ultra-strong coupling regime [17].

4. Operation as an Eletro-Optical Switch

The electro-optical functionality is realized by tuning the electron density of ITO N_{ITO} via applying a bias voltage. The hollow gold square and the ITO nanofilm shown in Fig. 1 are used as electrodes to achieve tunable electro-optical switching by introducing additional free electrons in ITO. Additional free electrons are accumulated in the cross-shaped ITO arrays and the ITO nanofilm to alter the optical response by shifting the plasma frequency ω_{p} in Eq. (2). The state-of-the-art multi-gate technology [36] in microelectronic industry, which is used to assume better control over the electric switching operation by increasing the surface area of voltage application, can also be used here to increase the thickness of the ITO accumulation layer and uniform the additional free electrons distribution. Fig. 7 shows that, with the decrease of the electron density of ITO, the ER of the short-wavelength dip becomes larger, and that of the short-wavelength dip becomes smaller. The electro-optical switch can achieve a modulation depth of 8 dB to ~17 dB from 1.375 μm to 1.545 μm by applying a bias voltage. Moreover, the switching between ON/OFF states, the modulation depth, and the working wavelength of the switch can be tuned by different N_{ITO}, as demonstrated in Fig. 8(a). When $N_{\mathrm{ITO}} = 1.06 \times 10^{21}$ cm^{-3}, light can pass through and have a transmission of

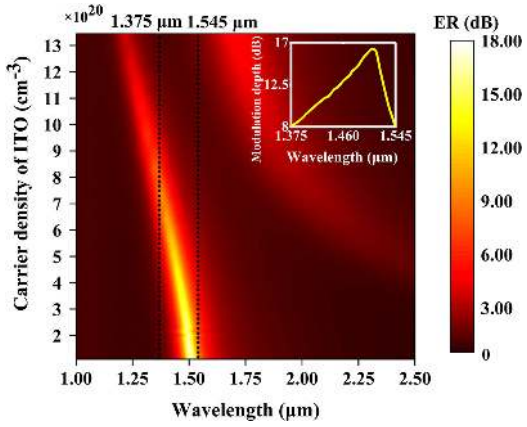

Fig. 7. The evolution of the transmission spectra of the tunable electro-optical switch as a function of N_{ITO}. The subfigure in top right corner is the modulation depth from 1.375 μm to 1.545 μm.

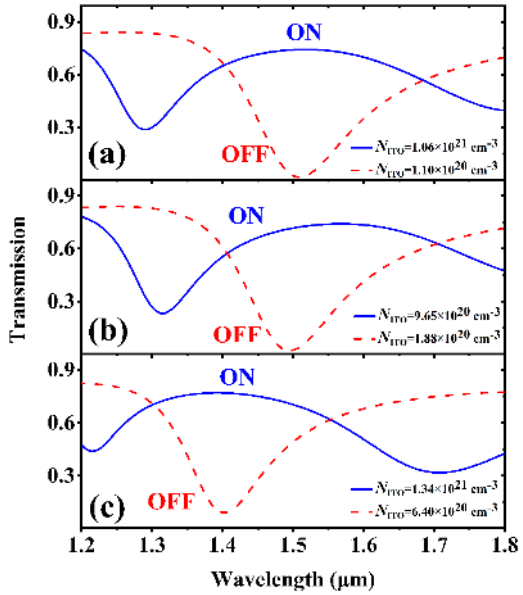

Fig. 8. The performance in tunable electric-optical switches. At ON state, (a) $N_{\mathrm{ITO}} = 1.06 \times 10^{21}$ cm^{-3}, (b) $N_{\mathrm{ITO}} = 9.65 \times 10^{20}$ cm^{-3}, and (c) $N_{\mathrm{ITO}} = 1.34 \times 10^{21}$ cm^{-3}. At OFF state, (a) $N_{\mathrm{ITO}} = 1.10 \times 10^{20}$ cm^{-3}, (b) $N_{\mathrm{ITO}} = 1.88 \times 10^{20}$ cm^{-3}, and (c) $N_{\mathrm{ITO}} = 6.40 \times 10^{20}$ cm^{-3}. The modulation depths are (a) 16.56 dB, (b) 15.33 dB, and (c) 9.4 dB at 1.51 μm, 1.49 μm, and 1.40 μm, respectively.

0.74 (1.29 dB) at 1.51 μm, which is the ON state. While when N_{ITO} is tuned to 1.10×10^{20} cm^{-3} via applying a different bias voltage, the corresponding transmission is 0.016 (17.85 dB), which corresponds to the OFF state. From Figs. 8(b) and 8(c), the switch exhibits a modulation depth of 15.33 dB and 9.4 dB at 1.49 μm and 1.40 μm, respectively.

5. Operation as an All-Optical Switch

On the other hand, the proposed device can be used as an all-optical switch. ENZ ITO can exhibit a large nonlinear response near its ENZ wavelength. The real part of the nonlinear complex refractive

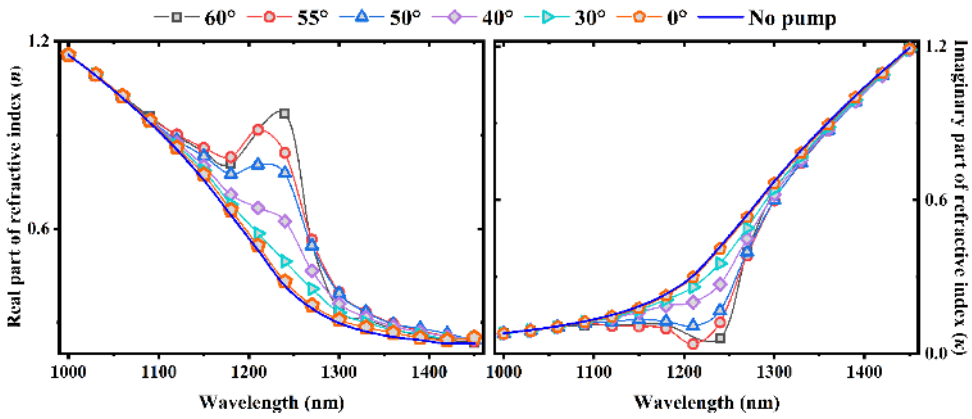

Fig. 9. The calculated real part (a) and the imaginary part (b) of the complex refractive index of ITO.

index of ITO can be expressed as [18], [37]:

$$n = n_0 + n_{2(\text{eff})} I, \tag{3}$$

here n_0 is the linear refractive index part of ITO before excitation by the pump beam of intensity I, and $n_{2(\text{eff})}$ is the effective nonlinear refractive index. The effective nonlinear absorption coefficient is defined as [18]:

$$\beta_{(\text{eff})} = \frac{\Delta\alpha}{I}, \tag{4}$$

where $\Delta\alpha$ is the change in attenuation constant induced by the pump beam of intensity I. The absorption coefficient α is given by [37], [38]:

$$\alpha = \frac{4\pi\kappa}{\lambda}, \tag{5}$$

where κ is the imaginary part of the complex refractive index of ITO. Based on the above formulae, we calculate the real part and the imaginary part of the complex refractive index of ITO at $I = 5$ GW/cm^2, as shown in Figs. 9(a) and 9(b). In the calculation, the effective nonlinear refractive index $n_{2(\text{eff})}$ and the effective nonlinear absorption coefficient $\beta_{2(\text{eff})}$ are obtained from Ref. [18]. The real part of the refractive index of ITO rises sharply and the imaginary part decreases near 1240 nm when the incident angle of the pump light increases from 0° to 60°. And this ultrafast reversible change in refractive index with a response time of about 650 fs. It can be expected that drastic changes in the complex refractive index of ITO will cause ultrafast changes in the optical response of the proposed structure.

Based on the mechanisms mentioned above, the tunable ultrafast all-optical switching of the proposed structure is demonstrated. As shown in Fig. 10(a), a pump light of intensity I is incident at an angle θ, to stimulate the nonlinear response near the ENZ wavelength of ITO. A probe light is normally incident on the structure, and the switching operation is controlled by the pump beam. With a pump light of $I = 5$ GW/cm^2, the transmission of the all-optical switch in Fig. 10(b) becomes larger when θ increases. The transmission spectra vary from 0.16 to 0.52, which corresponds to an ER exceeding 5 dB at 1240 nm. In addition, Fig. 10(c) reveals that increasing I results in a larger transmission. Thus, the all-optical switch can be controlled by the pump light incident angle and intensity. It is worth noting that the ER of the all-optical switch can be enhanced through applying a different bias voltage, making it a hybrid switch. For performance verification, the linear response of the metasurface can be measured by using a thermal light source and a custom-built transmittance measurement system, and the nonlinear response of the metasurface can be measured by using

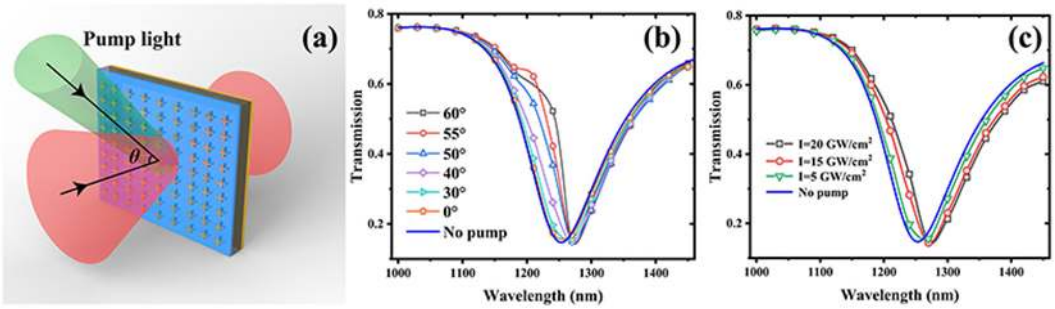

Fig. 10. (a) Schematic of the all-optical switch based on the proposed structure. A pump light of intensity I is incident at an angle θ, and a probe light is normally incident on the structure. The periodicity of the unit cell is set as $P_x = P_y = 750$ nm. (b) The transmission of the all-optical switch under different pump light incident angles θ, with an intensity $I = 5$ GW/cm^2. (c) Transmission at a different intensity I when $\theta = 30°$.

a single-beam *z*-scan technique and a regeneratively amplified femtosecond laser pumped optical parametric amplifier as the source laser [39].

6. Conclusions

We propose a tunable dual-function optical switch based on the ENZ metasurface. An obvious Rabi splitting with two dips is observed in the transmission spectrum by introducing the ENZ ITO material. It is found that the coupling between the ENZ mode and plasmon resonance gives rise to the Rabi splitting, by means of analyzing the field distributions of |E| and |H| of the short- and long-wavelength dips. The ENZ mode and the plasmon resonance play a leading role in the short- and long-wavelength dips, respectively. The numerical results also demonstrate that the coupled system in the proposed structure belongs to the ultra-strong coupling regime.

Additionally, the functionalities of tunable electro-optical switching and ultrafast all-optical switching are investigated based on the proposed optical design. The optical switch can be tuned by a bias voltage, the incident angle, and intensity of the pump light. When operating as an electro-optical switch, a modulation depth of 8 dB to ~17 dB from 1.375 μm to 1.545 μm can be achieved by applying a bias voltage. When functioning as an all-optical switch, an ER exceeding 5 dB with a response time of ~650 fs under the control of the pump light. Owing to these three flexible controlling dimensions, the proposed optical switch shows great application potential in ultrafast optical communication networks and integrated logical photonic circuits.

References

[1] Z. Chai, X. Hu, F. Wang, X. Niu, J. Xie, and Q. Gong, "Ultrafast All-Optical Switching," *Adv. Opt. Mater.*, vol. 5, no. 7, 2017, Art. no. 1600665.
[2] S. Fan, "Sharp asymmetric line shapes in side-coupled waveguide-cavity systems," *Appl. Phys. Lett.*, vol. 80, no. 6, pp. 908–910, 2002.
[3] A. Bazin *et al.*, "Ultrafast all-optical switching and error-free 10 Gbit/s wavelength conversion in hybrid InP-silicon on insulator nanocavities using surface quantum wells," *Appl. Phys. Lett.*, vol. 104, no. 1, 2014, Art. no. 011102.
[4] H. Lu, X. Liu, L. Wang, Y. Gong, and D. Mao, "Ultrafast all-optical switching in nanoplasmonic waveguide with Kerr nonlinear resonator," *Opt. Express*, vol. 19, no. 4, pp. 2910–2915, 2011.
[5] Z. L. Sámson *et al.*, "Metamaterial electro-optic switch of nanoscale thickness," *Appl. Phys. Lett.*, vol. 96, no. 14, 2010, Art. no. 143105.
[6] W. Luo *et al.*, "Flexible modulation of plasmon-induced transparency in a strongly coupled graphene grating-sheet system," *Opt. Express*, vol. 24, no. 6, pp. 5784–5793, 2016.
[7] M. Waldow *et al.*, "25ps all-optical switching in oxygen implanted silicon-on-insulator microring resonator," *Opt. Express*, vol. 16, no. 11, pp. 7693–7702, 2008.

[8] C. L. Wu *et al.*, "Enhancing optical nonlinearity in a nonstoichiometric SiN waveguide for cross-wavelength all-optical data processing," *ACS Photon.*, vol. 2, no. 8, pp. 1141–1154, 2015.
[9] P. Guo, R. D. Schaller, J. B. Ketterson, and R. P. H. Chang, "Ultrafast switching of tunable infrared plasmons in indium tin oxide nanorod arrays with large absolute amplitude," *Nature Photon.*, vol. 10, no. 4, pp. 267–273, 2016.
[10] R. W. Ziolkowski, "Propagation in and scattering from a matched metamaterial having a zero index of refraction," *Phys. Rev. E - Stat. Physics, Plasmas, Fluids, Relat. Interdiscip. Top.*, vol. 70, no. 4, 2004, Art. no. 046608.
[11] X. Niu, X. Hu, S. Chu, and Q. Gong, "Epsilon-near-zero photonics: A new platform for integrated devices," *Adv. Opt. Mater.*, vol. 6, no. 10, 2018, Art. no. 1701292.
[12] O. Reshef, I. De Leon, M. Z. Alam, and R. W. Boyd, "Nonlinear optical effects in epsilon-near-zero media," *Nature Rev. Mater.*, vol. 4, no. 8, pp. 535–551, 2019.
[13] I. Liberal and N. Engheta, "Near-zero refractive index photonics," *Nature Photon.*, vol. 11, no. 3, pp. 149–158, 2017.
[14] M. Silveirinha and N. Engheta, "Tunneling of electromagnetic energy through subwavelength channels and bends using ε-near-zero materials," *Phys. Rev. Lett.*, vol. 97, no. 15, 2006, Art. no. 157403.
[15] S. Enoch, G. Tayeb, P. Sabouroux, N. Guérin, and P. Vincent, "A metamaterial for directive emission," *Phys. Rev. Lett.*, vol. 89, no. 21, 2002, Art. no. 213902.
[16] Y. Jin, P. Zhang, and S. He, "Abnormal enhancement of electric field inside a thin permittivity-near-zero object in free space," *Phys. Rev. B - Condens. Matter Mater. Phys.*, vol. 82, no. 7, pp. 2–6, 2010.
[17] J. R. Hendrickson *et al.*, "Coupling of epsilon-near-zero mode to gap plasmon mode for flat-top wideband perfect light absorption," *ACS Photon.*, vol. 5, no. 3, pp. 776–781, 2018.
[18] M. Z. Alam, I. De Leon, and R. W. Boyd, "Large optical nonlinearity of indium tin oxide in its epsilon-near-zero region," *Sci. 352*, vol. 352, no. 6287, pp. 795–797, 2016.
[19] J. Wu, B. A. Malomed, H. Y. Fu, and Q. Li, "Self-interaction of ultrashort pulses in an epsilon-near-zero nonlinear material at the telecom wavelength," *Opt. Express*, vol. 27, no. 26, pp. 37298–37307, 2019.
[20] G. V. Naik, J. Kim, and A. Boltasseva, "Oxides and nitrides as alternative plasmonic materials in the optical range [Invited]," *Opt. Mater. Express*, vol. 1, no. 6, pp. 1090–1099, 2011.
[21] S. J. Kim and M. L. Brongersma, "Active flat optics using a guided mode resonance," *Opt. Lett.*, vol. 42, no. 1, pp. 5–8, 2017.
[22] A. Capretti, Y. Wang, N. Engheta, and L. Dal Negro, "Comparative study of second-harmonic generation from epsilon-near-zero indium tin oxide and titanium nitride nanolayers excited in the near-infrared spectral range," *ACS Photon.*, vol. 2, no. 11, pp. 1584–1591, 2015.
[23] T. S. Luk *et al.*, "Enhanced third harmonic generation from the epsilon-near-zero modes of ultrathin films," *Appl. Phys. Lett.*, vol. 106, no. 15, pp. 1–6, 2015.
[24] T. S. Luk *et al.*, "Directional perfect absorption using deep subwavelength low-permittivity films," *Phys. Rev. B - Condens. Matter Mater. Phys.*, vol. 90, no. 8, pp. 1–10, 2014.
[25] M. Kelley, A. Lee, M. Mozumdar, K. Dajani, and A. Ahmed, "Design and modeling of subpicosecond all-optical modulator using the nonlinear response of indium tin oxide," *J. Opt. Soc. Amer. B*, vol. 36, no. 8, pp. F149–F153, 2019.
[26] Z. Chai *et al.*, "Ultrafast on-chip remotely-triggered all-optical switching based on epsilon-near-zero nanocomposites," *Laser Photon. Rev.*, vol. 11, no. 5, 2017, Art. no. 1700042.
[27] Q. Guo *et al.*, "A solution-processed ultrafast optical switch based on a nanostructured epsilon-near-zero medium," *Adv. Mater.*, vol. 29, no. 27, 2017, Art. no. 1700754.
[28] X. Jiang, H. Lu, Q. Li, H. Zhou, S. Zhang, and H. Zhang, "Epsilon-near-zero medium for optical switches in a monolithic waveguide chip at 1.9 μm," *Nanophotonics*, vol. 7, no. 11, pp. 1835–1843, 2018.
[29] L. Jin, Q. Chen, W. Liu, and S. Song, "Electro-absorption modulator with dual carrier accumulation layers based on epsilon-near-zero ITO," *Plasmonics*, vol. 11, no. 4, pp. 1087–1092, 2016.
[30] S. A. Maier, *Plasmonics: Fundamentals and Applications*. Berlin, Germany: Springer Science & Business Media, 2007.
[31] S. Campione, S. Liu, A. Benz, J. F. Klem, M. B. Sinclair, and I. Brener, "Epsilon-near-zero modes for tailored light-matter interaction," *Phys. Rev. Appl.*, vol. 4, no. 4, 2015, Art. no. 044011.
[32] S. Campione, I. Brener, and F. Marquier, "Theory of epsilon-near-zero modes in ultrathin films," *Phys. Rev. B - Condens. Matter Mater. Phys.*, vol. 91, no. 12, 2015, Art. no. 121408.
[33] S. A. Schulz, A. A. Tahir, M. Z. Alam, J. Upham, I. De Leon, and R. W. Boyd, "Optical response of dipole antennas on an epsilon-near-zero substrate," *Phys. Rev. A*, vol. 93, no. 6, 2016, Art. no. 063846.
[34] L. Novotny, "Effective wavelength scaling for optical antennas," *Phys. Rev. Lett.*, vol. 98, no. 26, 2007, Art. no. 266802.
[35] J. Dintinger, S. Klein, F. Bustos, W. L. Barnes, and T. W. Ebbesen, "Strong coupling between surface plasmon-polaritons and organic molecules in subwavelength hole arrays," *Phys. Rev. B - Condens. Matter Mater. Phys.*, vol. 71, no. 3, 2005, Art. no. 035424.
[36] I. Ferain, C. A. Colinge, and J. P. Colinge, "Multigate transistors as the future of classical metal-oxide-semiconductor field-effect transistors," *Nature*, vol. 479, no. 7373, pp. 310–316, 2011.
[37] R. W. Boyd, *Nonlinear Optics*. Amsterdam, The Netherlands: Elsevier, 2003.
[38] M. Fox, *Optical Properties of Solids*. Baltimore, MA, USA: American Association of Physics Teachers, 2002.
[39] M. Z. Alam, S. A. Schulz, J. Upham, I. De Leon, and R. W. Boyd, "Large optical nonlinearity of nanoantennas coupled to an epsilon-near-zero material," *Nature Photon.*, vol. 12, no. 2, pp. 79–83, 2018.